

Pulsars identified in the LOFAR Two-metre Sky Survey at 144 MHz

G. A. C. Rijkers¹, C. G. Bassa², J. R. Callingham^{2,3}, and T. Shimwell^{2,1}

¹ Leiden Observatory, Leiden University, P.O. Box 9500, 2300 RA Leiden, The Netherlands
e-mail: rijkers@strw.leidenuniv.nl

² ASTRON, Netherlands Institute for Radio Astronomy, Oude Hoogetveensedijk 4, 7991 PD Dwingeloo, The Netherlands

³ Anton Pannekoek Institute for Astronomy, University of Amsterdam, Science Park 904, 1098 XH Amsterdam, The Netherlands

Received September 29, 2025; Accepted December 8, 2025

ABSTRACT

We present the astrometric identification of 80 known radio pulsars as unresolved continuum sources detected at 144 MHz in the second data release of the LOFAR Two-metre Sky Survey (LoTSS DR2), which covers 27% of the Northern hemisphere. These identifications represent the majority ($\geq 86\%$) of radio pulsars present in the LoTSS DR2 footprint and provide independent celestial positions and flux densities at 144 MHz. We compare LoTSS flux densities with literature values from various image and time-domain observations and find good agreement for all but two pulsars. We attribute these flux density deviations to intrinsic pulsar properties (nulling and off-pulse emission). We investigate criteria to select promising pulsar candidates using data from the upcoming LoTSS release of the entire Northern sky ($\delta > 0^\circ$), as well as the LOFAR LBA Sky Survey (LoLSS) at 54 MHz (covering $\delta > 24^\circ$). Of the 80 detections, 35 (44%) were blindly redetected based on their linear or circular polarization. Therefore we conclude that candidate selection based on polarization properties is a promising approach. Candidate selection can be supplemented with spectral indices via cross-matching to LoLSS sources at 54 MHz, as the high sensitivity of LoTSS is not matched by image-domain surveys at higher frequencies.

Key words. catalogs – pulsars: general – radio continuum: general

1. Introduction

By nature of their regular pulsations, radio pulsars offer unique probes into various astrophysical processes through the method of pulsar timing (see review by [Stairs 2003](#)). These processes range from measuring neutron star properties (e.g. [Fonseca et al. 2021](#); [Keith et al. 2024](#)), understanding the properties of the interstellar medium (e.g. [Sobey et al. 2019](#); [Main et al. 2023](#)), constraining nano-Hertz gravitational waves (e.g. [Afzal et al. 2023](#); [EPTA Collaboration et al. 2023](#); [Reardon et al. 2023](#); [Xu et al. 2023](#)) and characterizing the Galactic population of pulsars, and with it, that of neutron stars (e.g. [Faucher-Giguère & Kaspi 2006](#); [Graber et al. 2024](#)). These results are predicated on the necessity to resolve the pulsar pulse profile, hence high-time resolution radio observations are required to resolve pulsations for even the fastest spinning radio pulsars (which have spin periods as fast as to $P = 1.4$ ms; [Hessels et al. 2006](#); [Bassa et al. 2017](#)).

Interferometric observations using aperture synthesis ([Jennison 1958](#); [Ryle & Hewish 1960](#)) generally trade time resolution for spatial resolution and hence fully integrate over the pulse profile of pulsars. These phase averaged observations provide independent measurements of pulsar flux densities, polarization properties and celestial positions, and are not biased by temporal smearing of the pulse profile by dispersion and scatter broadening, which are strongly dependent on the pulsar spin period and the pulsar dispersion measure ([Cordes & McLaughlin 2003](#)), as well as any temporal smearing due to unresolved binary motion ([Ransom et al. 2002](#)). Additionally, the flux scale in imaging observations is better defined than that of high time resolution single dish observations of beamformed observations with multi-element telescopes, which need to rely on accurate knowledge of instrumental param-

eters through the radiometer equation (e.g. [Lorimer & Kramer 2004](#)). As a result, wide-area imaging surveys provide uniform flux density measurements for large fractions of the pulsar population.

Conversely, radio pulsars typically have steep radio spectra ($S_\nu \propto \nu^\alpha$ with $\alpha = -1.6 \pm 1.0$; [Jankowski et al. 2018](#)), and significant linear or circular polarization fractions ([Posselt et al. 2023](#)) which allows for identification of radio pulsar candidates from imaging observations. This point is perhaps best illustrated by the discovery of the first radio millisecond pulsar PSR B1937+21 ($P = 1.6$ ms) by [Backer et al. \(1982\)](#), which was found by targeting the steep spectrum, strongly scintillating and linearly polarized point source 4C21.53¹.

In this paper we search for known radio pulsars that are present in the LOFAR Two-metre Sky Survey (LoTSS; [Shimwell et al. 2017](#)) as continuum sources. LoTSS is an ongoing radio continuum survey of the Northern hemisphere at frequencies between 120 and 168 MHz with LOFAR ([van Haarlem et al. 2013](#)). The survey reaches sensitivities of $100 \mu\text{Jy beam}^{-1}$ at a resolution of $6''$. The majority of pointings have an integration time of at least 8 hours. The latest LoTSS data release (DR2; [Shimwell et al. 2022](#)) provides total intensity images and a catalog containing more than 4 million sources for 27% of the Northern hemisphere, mostly at high Galactic latitudes ($|b| > 15^\circ$).

In Sect. 2 we cross match the LoTSS DR2 catalog to astrometric positions of radio pulsars. The resulting detections and non-detections are discussed in Sect. 3, which provides flux density measurements, polarization properties and an investigation

¹ The history of this discovery has recently been recollected by [Readhead \(2024\)](#); [Demorest & Goss \(2024\)](#) and [Kulkarni \(2024\)](#).

of globular cluster environments. We discuss and conclude in Sect. 4, where we focus on the number of radio pulsars detected in LoTSS, compare flux density measurements from image and time-domain methods, discuss selection criteria for identifying pulsar candidates, and present an outlook for upcoming LOFAR image domain data releases.

2. Catalog cross-matching

We use the ATNF pulsar catalog (PSRCAT; Manchester et al. 2005)², which collates pulsar properties from the literature. We used version v2.2.0 which contains properties of 3630 pulsars, of which the majority are spin-powered radio pulsars, though the catalog also includes X-ray and gamma-ray emitting pulsars and magnetically powered magnetars. The pulsar catalog provides rotational, astrometric properties, as well as binary parameters for those pulsars in binaries.

We amend the pulsar catalog with information from recent publications. These include timing solutions for 16 pulsars discovered with LOFAR from van der Wateren et al. (2023), four Fermi γ -ray pulsars (three by Abdollahi et al. 2022, one by Smith et al. 2023), one pulsar discovered as part of the Green Bank North Celestial Cap (GBNCC) survey (Fiore et al. 2023), one CHIME pulsar (Dong et al. 2023) and one pulsar discovered with the Large Phased Array telescope by Tyul'bashev et al. (2017). We also use LOFAR timing solutions for six pulsars by McKenna et al. (2024) and McKenna (2024). For PSR J1641+3627F in the globular cluster M13, the updated values from the FAST timing solution (Wang et al. 2020) did not contain an uncertainty value in declination, and we assume it to be in the last significant digit; $\sigma_\delta = 0''.0010$. For PSR J2212+2450 we use the recent timing position from Lewis et al. (2023).

Proper motion is accounted for when available in PSRCAT, using the reported position epoch in PSRCAT and the observation date of the LoTSS observation. In the case where a pulsar overlaps with more than one LoTSS observation, we use the observation whose pointing is closest to the location of the pulsar. For those pulsars that have a known proper motion, it is only applied when there is also a known uncertainty on the proper motion. In general, the positional shifts due to proper motion were negligible ($0''.05$ or less), except for PSRs B1112+50 at $1''.14$, B1508+55 at $1''.28$ and J1605+3249 at $2''.43$, as these pulsars have high proper motion and/or positional epochs from the early 2000s.

We find that 117 pulsars in the pulsar catalog are located within the sky area surveyed in LoTSS DR2. Positional uncertainties are not available in PSRCAT for 10 pulsars, and for 13 other pulsars the positional uncertainties exceed $20''$ in one or both coordinates, precluding unique identification of pulsar counterparts. These pulsars are removed from our sample, and the total number of pulsars with reliable information that we can cross-match to LoTSS sources is 95.

For these 95 pulsars, we use the positional information to compute 99% confidence uncertainty regions to identify counterparts in the LoTSS DR2 catalog and images. Here, the positional uncertainties in right ascension and declination of pulsars are summed in quadrature with the positional uncertainty in the frame tie of LoTSS to the ICRS. The frame tie is estimated at $0''.20$ in both right ascension and declination based on optical-radio matches (Shimwell et al. 2022). The typical value for the positional uncertainty of LoTSS sources is also added in

the quadratic sum, for which we take the median positional uncertainty of $\sim 0''.50$ in either coordinate for LoTSS sources with fluxes between 0.1 and 10 mJy.

The 99% uncertainty regions are a factor $[-2\log_e(1 - 0.99)]^{1/2} = 3.035$ larger than the total 1σ uncertainties in either coordinate. We consider LoTSS sources coincident within the 99% confidence pulsar uncertainty regions as counterparts.

3. Results

3.1. Detections

For the 95 pulsars with accurate positional information, we find that 80 pulsars have a LoTSS counterpart. Among those pulsars, 76 have a LoTSS source coincident with the 99% confidence uncertainty regions. Visual inspection of the LoTSS images of all 95 pulsars reveal four further matches which are discussed below. The properties of the radio pulsars and their associated LoTSS sources are given in Table A.1, and pulsar positions are overlaid on LoTSS continuum images for 9 pulsars in Fig. 1.

Given the LoTSS source density of 0.22 sources per square arcminute, we estimate the number of unrelated LoTSS sources coincident with one of the 99% confidence uncertainty regions of all pulsars (covering 2.64 square arcminutes in total) at 0.6, suggesting that on the order of one pulsar may be associated with a LoTSS source due to random chance. Excluding the four pulsars matched by visual inspection, we find that the average offset between the pulsar positions and the LoTSS source positions is consistent within the uncertainties ($\Delta\alpha = 0''.19 \pm 0''.94$ and $\Delta\delta = -0''.02 \pm 0''.94$). The cumulative density function (CDF) positional offsets we measure correspond to a Rayleigh distribution with a scale parameter of $\sigma = 0.61$. A value near unity is expected for σ , which shows that the positional uncertainties are likely overestimated. Neglecting the uncertainties in the frame-tie, which are systematic and not random, yields $\sigma = 1.30$, while decreasing the frame-tie uncertainty to $0''.05$ in both coordinates results in $\sigma = 1.05$. This leads us to conclude that our sample of matches is statistically complete.

Four sources were visually matched to pulsars.

B1112+50: Due to its location in the wings of the point-spread function of a brighter source (ILT J11538.50+503023.8, $S_{144} = 233$ mJy) located $13''$ North of the pulsar position, PSR B1112+50 is detected in LoTSS imaging, but catalogued as an extended and offset source. The proximity of the pulsar and the brighter source appears to have impacted the LoTSS source finding algorithm, as the source positions and source extent are deviating from the peaks in the image (Fig. 1i). We note that O'Sullivan et al. (2023) matched PSR B1112+50 with the brighter source ILT J11538.50+503023.8. This misidentification was also made by Frail et al. (2016) due to the lower angular resolution of the TGSS survey, as they report a flux density (198 mJy), far higher than the peak flux in LoTSS ($S_{144} = 21$ mJy) and other literature. Based on NVSS observations at 1.4 GHz, Kaplan et al. (1998) mentions that the matching of PSR B1112+50 was confused by a source $12''$ away, which is consistent with our observations.

J0227+3356: Two point sources of similar brightness have been identified as a single extended source in the LoTSS catalog (Fig. 1f). The coincidence of the pulsar with one of the two indicates that these sources are not related to each other, and that the Southern source is the LoTSS counterpart to PSR J0227+3356.

J1336+3414: In two separate LoTSS pointings, P204+32 and P204+35, there is a clear patch of emission at the location of PSR J1336+3414 (Fig. 1e) though no source has been catalogued

² www.atnf.csiro.au/research/pulsar/psrcat/

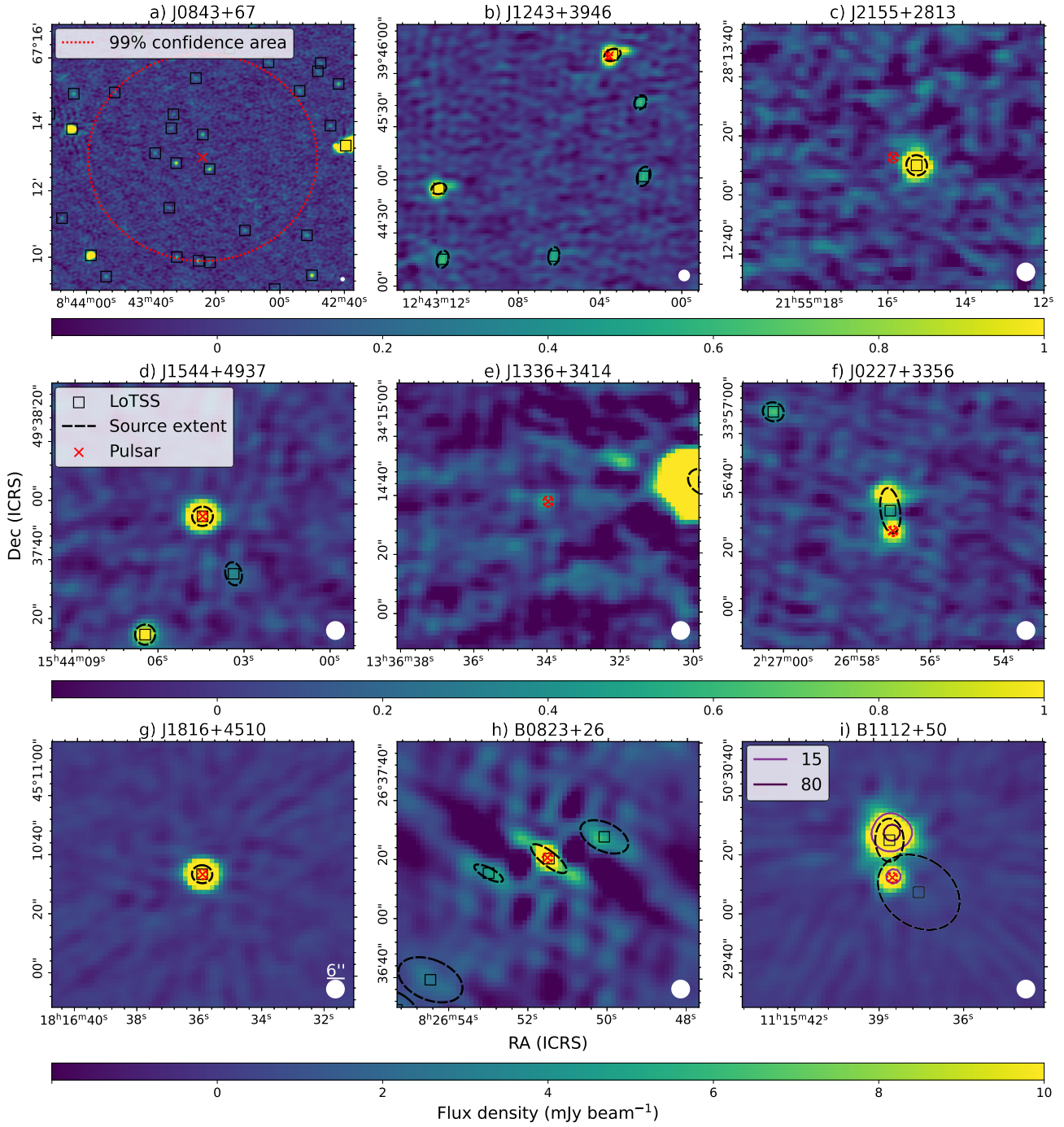


Fig. 1. LoTSS DR2 images in Stokes I for nine example pulsars. All images have a field-of-view of $90'' \times 90''$, except for panel a) which has $8' \times 8'$ and panel b) which has 2.5×2.5 . Positions of LoTSS sources are indicated with a black square, while positions from the pulsar catalog are denoted with the red cross. The extent of LoTSS sources is shown with the black dashed ellipses, depicting the major- and minor axes resulting from fitting to the LoTSS sources (Shimwell et al. 2022). The FWHM of the LoTSS beam is shown in the bottom-right corners. Flux density contours in mJy beam^{-1} are plotted for panel i) to highlight the structure within bright sources. Panel d) and g) show example pulsars with accurate position measurements, leading to a unique match to a LoTSS source, while panel a) shows an example where the positional uncertainty of the pulsar is large and several LoTSS sources coincide with the 99% confidence error region (denoted by the red dotted ellipse). In panel b) a field of LoTSS sources are shown, where the Northern-most source is matched to a pulsar. All visible components show source extension to the East, indicating an imaging problem. Pulsar J1336+3414 is dimly visible as a point source in panel e), and due to its low brightness and/or the proximity of the Eastern bright source it is a $\sim 4\sigma$ detection that is not catalogued in LoTSS DR2. We estimate its flux density directly from the image. Panel c) shows a pulsar with a separation of $8.4'$ to a LoTSS source, but does not contain it within its 99% uncertainty ellipse. In panel f) a pulsar is matched to a LoTSS source that was classified as a single extended object, while in fact consists of two unrelated objects, one of which is the pulsar counterpart. Finally, panel i) shows a compact radio source that is present at the position of PSR B1112+50, but due to the proximity of a brighter radio source, it is catalogued in LoTSS as an extended source with an offset position.

in LoTSS. A flux density of ~ 0.5 mJy is measured for the pulsar. This flux is a $\sim 4\sigma$ detection, which together with the perturbing nearby source, explains the absence of the pulsar in the LoTSS catalog.

J2155+2813: This pulsar is offset by $8''.4$ from the 4.7 mJy LoTSS source ILT J215515.22+281309.3. While this is well outside the 99% confidence error region of the pulsar based on the pulsar timing position by [Lewandowski et al. \(2004\)](#), the similarity between the LoTSS flux density and those obtained from earlier LOFAR time-domain observations ([Sanidas et al. 2019](#) at 4.8 ± 2.2 mJy and [Bilous et al. 2016](#) at 9.6 ± 4.8 mJy), the absence of another radio source at the pulsar position, and the absence of multi-wavelength counterparts in WISE/Panstarss at either location, leads us to consider ILT J215515.22+281309.3 as the counterpart to PSR J2155+2813. Future timing observations would have to confirm whether the timing ephemeris of [Lewandowski et al. \(2004\)](#) is in error. We rule out proper motion, because the known distance to the pulsar ([Lewandowski et al. 2004](#), [Manchester et al. 2005](#)) would imply an unrealistically high tangential velocity.

Two sources showed anomalies in the images:

B0823+26: This pulsar is surrounded by clear imaging artifacts (Fig. 1h) that are not seen around other nearby sources in this LoTSS pointing. We hypothesise that these artifacts are caused by the intermittent behaviour (nulling) of the pulsar. The pulsar is known to turn on/off on a timescale of minutes and hours ([Young et al. 2012](#), [Sobey et al. 2015](#)), which is on the same scale as the exposure time. We expect that due to the intermittent behaviour, the UV-coverage for this source is incomplete, which conflicts with the assumption of continuous emission of the CLEAN algorithm, leading to imaging artifacts (the surrounding bright spots) and the elliptical shape of the pulsar (Fig. 1h). Analysis of the visibilities at higher time resolution could confirm this hypothesis. Furthermore, the flux density we measure is an order of magnitude lower than was measured at 150 MHz in the literature ([Bilous et al. 2016](#), [Frail et al. 2016](#), [Sanidas et al. 2019](#)). If the pulsar was not emitting as often during the LoTSS observation as it did during the literature observations, that would explain this discrepancy.

J1243+3946: The counterpart to PSR J1243+3946 has an extension towards the East. Since all sources in the vicinity of the pulsar have this extension (Fig. 1b), we attribute this to an issue with the direction dependent phase- calibration of this pointing.

Lastly, we note that the LoTSS positions of PSRs J0006+1834, B0153+39, J1059+6459 and J2355+2246 improve upon values available in the pulsar catalog, which have positional uncertainties of order $1''$.

3.2. Non-detections

We did not find matches for 15 of 95 pulsars with accurate positions in v2.2.0 of the ATNF pulsar catalog. In this section, we discuss on an individual basis why we do not detect them.

For two pulsars, no radio emission is expected, as PSR J1605+3249 is the X-ray dim isolated neutron star RX J1605.3+3249 ([Haberl 2007](#)), for which no radio emission has yet been detected (e.g. [Kondratiev et al. 2009](#)), while PSR J1627+3219 is a millisecond pulsar associated with γ -ray source 4FGL J1627.7+3219 and detected through γ -ray pulsations and has no radio detection ([Smith et al. 2023](#)).

Six known radio pulsars in the globular clusters M3 (PSRs J1342+2822B and D) and M13 (PSRs J1641+3627C-F) are also not detected in LoTSS-DR2 imaging. As these pulsars have been discovered through deep targeted periodicity surveys,

the sensitivity limits are significantly deeper than those of wide-field untargeted surveys. This is confirmed by the flux density measurements at 1400 MHz for 5 of these pulsars from the pulsar catalog, which are in the range of 0.01 to 0.03 mJy. Assuming a power-law spectra with $\alpha = -1.6$, this would yield $S_{144} \approx 0.4$ to 1.1 mJy and close to the LoTSS detection threshold.

There are 4 radio emitting pulsars (PSRs J0211+4235, J1048+5349 J1502+4653 and J2307+2225) which could be detected in LoTSS imaging.

J0211+4235: The pulsar was discovered with FAST ([Wu et al. 2023](#)) and a flux density of $109 \mu\text{Jy}$ was reported at 1.25 GHz. Given the 5σ rms noise of 0.5 mJy at 144 MHz at the location of the pulsar, this constrains the spectral index of the source to $\alpha \geq -0.7$ assuming a power law spectrum.

J1502+4653: This pulsar was discovered with FAST ([Cruces et al. 2021](#)) at 1.36 GHz. With the given system specifications in [Cruces et al. \(2021\)](#), the integration time for PSR J1502+4653 and the radiometer equation, we estimate that the 5σ sensitivity of the FAST observation was $23.5 \mu\text{Jy}$. This constrains the spectral index to $\alpha \geq -1.4$ for a power law spectrum.

J1048+5349: This pulsar has been detected with the CHIME/Pulsar system ([CHIME/Pulsar Collaboration et al. 2021](#)), which has a minimum flux density limit of 0.6 mJy in the frequency range of 400 \sim 800 MHz ([Dong et al. 2023](#)). Given this minimum sensitivity, we would expect to detect this pulsar with LoTSS imaging for a large range of spectral indices.

J2307+2225: This pulsar has previously been detected in LOFAR time-domain observations ([Bilous et al. 2016](#)), hence we expected to detect the pulsar in LoTSS imaging. At 149 MHz its flux density is 0.9 ± 0.7 mJy, which is above the detection limit of LoTSS. Upon visual inspection, we do not detect a low-significance, uncatalogued source in LoTSS images. Continued timing observations with the Lovell telescope (B. Stappers et al., private communication) confirm that the values in PSRCAT are accurate.

The final three known radio pulsars (PSRs J0139+3326, J1006+3015 and J2237+2828) that have not been detected in LoTSS-DR2 imaging are known Rotating Radio Transients (RRATs; [McLaughlin et al. 2006](#); [Keane & McLaughlin 2011](#)); these pulsars are detected by occasional individual pulses instead of periodic emission and hence will have low integrated flux densities that are likely below the LoTSS detection limit.

J0139+3326: Detections of single pulses from this RRAT have been reported by [Tyul'bashev et al. \(2018\)](#), were followed up in [Brylyakova & Tyul'bashev \(2021\)](#) and later detected by [Sanidas et al. \(2019\)](#) as well. According to [Sanidas et al. \(2019\)](#), the pulsar has an estimated flux density at 135 MHz of 3.6 mJy, which is above the detection threshold of LoTSS, yet we do not detect it. As reported by [Michilli et al. \(2020\)](#), the RRAT only sporadically emits single pulses, without a periodic signal that can be distinguished from noise.

J1006+3015: The pulsar has been detected before by [Smirnova et al. \(2022\)](#), and by [McKenna et al. \(2024\)](#) using Irish LOFAR. The pulsar emits bright pulses on the order of 1 hr^{-1} , which are likely to be averaged out by the long observation time of LoTSS. This is confirmed by ongoing, preliminary, analysis of the 8 s LoTSS sub-integrations, which reveal 8 detections over the 8 hr observation (S. Ranguin and R. Thomas, private communication).

J2237+2828: The pulsar was discovered with ~ 70 hours of observation using CHIME ([Dong et al. 2023](#)) and was also detected by [McKenna et al. \(2024\)](#). It has been measured to emit bright pulses on the order of $1 \sim 2$ hours by [Dong et al. \(2023\)](#)

and Turner et al. (2025), while no fainter pulses have been detected.

3.3. Flux densities

The flux densities listed in Table A.1 expand upon the flux densities present in the literature. For 7 pulsars, image-domain flux densities at 150 MHz are available from Frail et al. (2016). Additionally, Sobey et al. (2022) presented flux density measurements for 6 pulsars, but since these based on pre-publication LoTSS observations, they are identical to those presented here. There are time-domain flux density measurements available in the literature at or around observing frequencies of 150 MHz for 58 out of 80 pulsars detected with LoTSS. The literature fluxes are as follows: measurements from LOFAR observations as part of the normal pulsar and millisecond pulsar censuses by Bilous et al. (2016) and Kondratiev et al. (2016, both at 150 MHz), redetected pulsars as part of the LOTAAS survey (Sanidas et al. 2019, at 135 MHz), and measurements from timing observations of pulsars discovered in LOTAAS (Tan et al. 2020; Michilli et al. 2020; van der Wateren et al. 2023, at 150 MHz, where we take the average of the 129 and 167 MHz measurements).

In general, the LoTSS flux densities are consistent with literature values for the majority of pulsars, see Fig. 2. Clear outliers are PSR B0823+26, which is a known nulling pulsar and for which measurements are available by Frail et al. (2016); Bilous et al. (2016) and Sanidas et al. (2019), and PSR J0218+4232, which has a matching flux density with Frail et al. (2016) but a large difference compared to Kondratiev et al. (2016). For 5 of the LOTAAS redetections the time-domain flux densities are at least $2\times$ brighter or fainter than the LoTSS values. Since the LOTAAS flux densities are determined from search observations whose pointings were offset from the pulsar positions, Sanidas et al. (2019) used a simple beam model to correct the observed flux densities. For 3 of the 5 pulsars the pointing offset was considerable (at least 2 beamwidths), which may explain the differences. For the 2 remaining LOTAAS redetections (PSRs J0944+4106 and J1059+6459) the pointing offsets are smaller, and we note that GBNCC observations at 350 MHz by Lynch et al. (2018) indicate these pulsars may display nulling.

3.4. Pulsars in polarized emission

The LoTSS DR2 survey observations have been used to search for radio sources with polarized emission. O’Sullivan et al. (2023) detected 2461 linearly polarized radio sources, of which 25 were matched to known radio pulsars, while Callingham et al. (2023) detected 68 circularly polarized sources, with 24 being matched to known radio pulsars. A total of 12 radio pulsars are detected in both linear and circular polarization by O’Sullivan et al. (2023) and Callingham et al. (2023). We compare these polarized detections to our sample of 80 known radio pulsars detected in the LoTSS survey through total intensity (Stokes I). We note that the pre-publication catalogues of O’Sullivan et al. (2023) and Callingham et al. (2023) were input to the work of Sobey et al. (2022) that led to the discovery of new radio pulsars or independent re-discoveries of known but poorly localized radio pulsars using targeted pulsation searches of unidentified polarized point sources. These pulsars are included in this analysis as well as those of O’Sullivan et al. (2023) and Callingham et al. (2023).

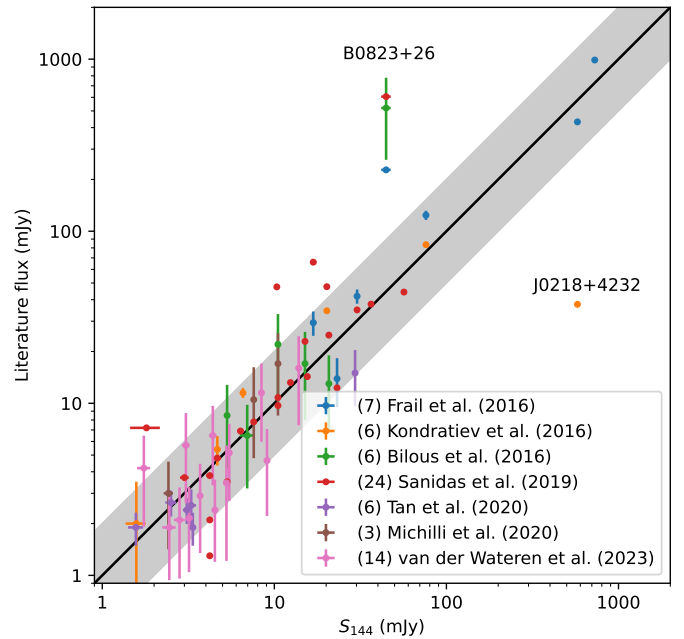


Fig. 2. Comparison of LoTSS flux densities from Table A.1 at 144 MHz (horizontal) to 150 MHz flux density measurements from image-domain observations by Frail et al. (2016) and time-domain observations by Bilous et al. (2016); Kondratiev et al. (2016); Tan et al. (2020); Michilli et al. (2020); van der Wateren et al. (2023) and Sanidas et al. (2019) at 135 MHz. The grey region represent fluxes ratios between factors 0.5 and 2.

All 25 linearly polarized pulsars identified by O’Sullivan et al. (2023) are also identified in LoTSS DR2 Stokes I images, though PSR B1112+50 has been mis-identified with the bright source offset and unrelated to the pulsar (further elaborated upon in Sect. 3.1). In the case of the 24 circularly polarized pulsars from Callingham et al. (2023), all but one are identified in LoTSS DR2, with the exception of PSR J0742+4110 which is not in the LoTSS DR2 Stokes I footprint. The known radio pulsars also identified from their polarized properties are marked in Table A.1.

As a result, of the 80 pulsars detected in total intensity, 35 stand out due to their polarization properties. As the detection of polarized emission depends both on the polarization fraction and the Stokes I flux density, detecting fainter sources through polarization is less likely. Pulsars have an average of 20% and 10% absolute linear and circular polarization fractions, respectively (Lorimer & Kramer 2012). Hence, an average pulsar needs a brightness of $S_{144} \geq 2.5 - 5.0$ mJy to be detected in the respective polarizations, which matches what we observe in our sample (2.0 mJy for linear and 4.9 mJy for circular). If we conservatively limit our sample to Stokes I flux densities of $S_{144} \gtrsim 4$ mJy, we find that 34 out of 51 pulsars (67%) are detectable through their polarization properties, with approximately equal fractions of either linear or either circular or both linear and circular polarization. We note that the bright millisecond pulsar PSR J0218+4232 ($S_{144} = 577$ mJy) was not detected as a polarized source by O’Sullivan et al. (2023) or Callingham et al. (2023), while it has previously been reported to have a linear polarization fraction of 40% (Navarro et al. 1995) up to 48% (Sobey et al. 2022), which far exceeds the detection limit of O’Sullivan et al. (2023). The high brightness of PSR J0218+4232 likely caused artificial polarized sources, which prevent its detection. Similarly, PSR J0815+4611 is not detected by O’Sullivan et al. (2023). The

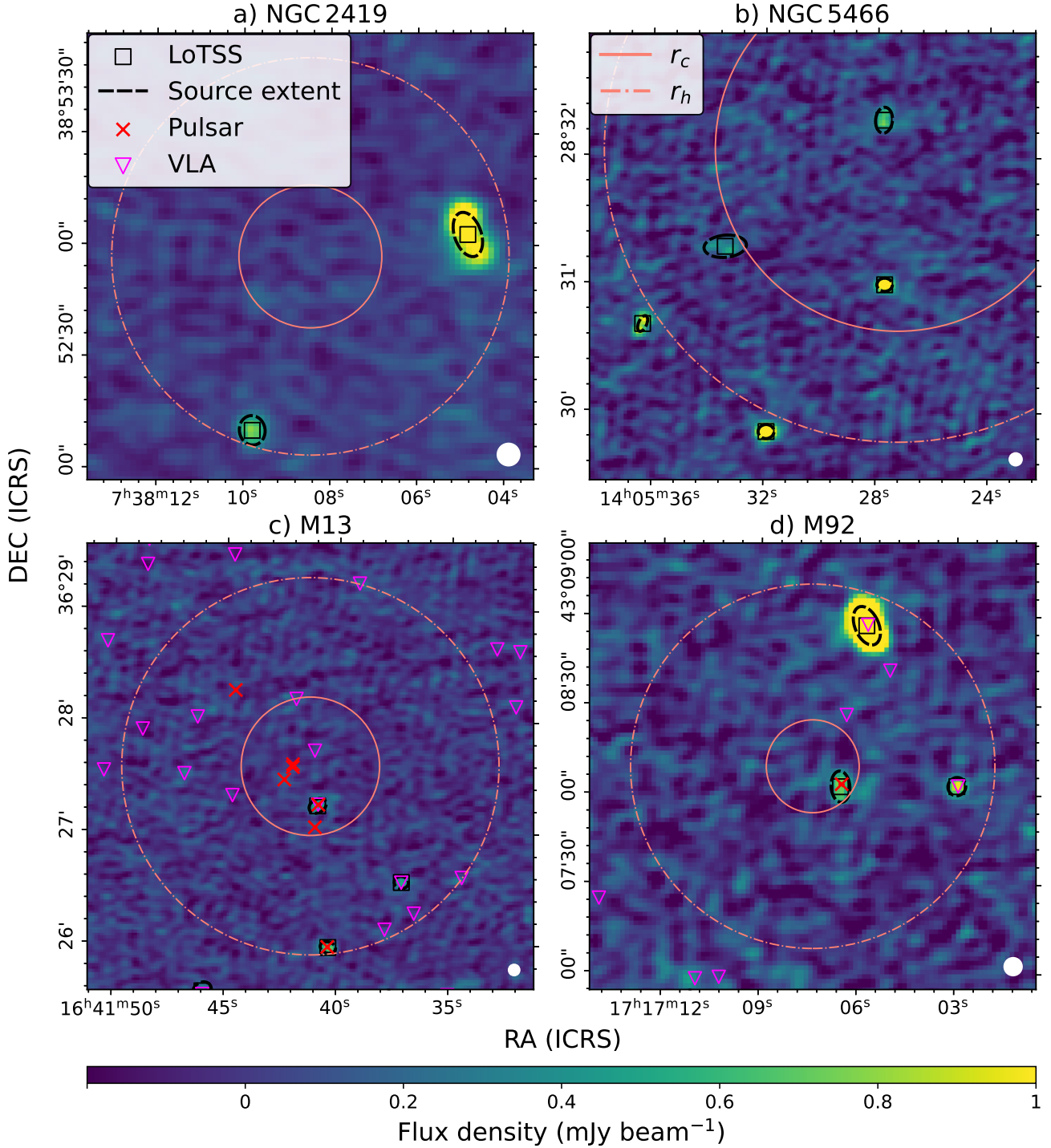


Fig. 3. LoTSS DR2 images in Stokes I for 7 globular clusters. The image in panel a) has a field-of-view of $2' \times 2'$. Panel b) has a field-of-view of $3.5' \times 3.5'$, and panels c) and d) have a field-of-view of $2.5' \times 2.5'$ and $4' \times 4'$ respectively. Positions of LoTSS sources are indicated with a black box, pulsar positions are denoted with the red cross and positions of VLA sources (Shishkovsky et al. 2020) are shown with magenta triangles. The core- and half-light radii of globular clusters are plotted in salmon with solid and dash-dotted circles respectively. The FWHM of the synthesized LoTSS beam of $6'' \times 6''$ is shown in the bottom-right corners.

pulsar has a linear polarization fraction of $\sim 50\%$ (Jelić et al. 2015) which translates to a flux density of twice the detection limit. Comparable to PSR J0218+4232, nearby bright sources could be causing artifacts that perturb the detection of PSR J0815+4611.

3.5. Globular Clusters

Radio (millisecond) pulsars are abundantly present in the dense stellar environments of globular clusters due to the combined effect of high stellar encounter rates and mass segregation where neutron stars tend to move to the cluster center. As a result, neu-

tron stars can be repeatedly spun up by mass transfer from one or more binary companions (e.g. [Verbunt & Freire 2014](#)).

The 2010 version of the [Harris \(1996\)](#) globular cluster catalog shows that the LoTSS DR2 footprint includes 7 Galactic globular clusters; M3, M13, M92, Ko 2, Pal 4, NGC 2419 and NGC 5466. Radio pulsars are known in M3, M13 and M92, with 6 in M3, of which 2 have accurate positions, but none are detected in LoTSS DR2. M13 has 6 pulsars, all with accurate positions of which 2 are detected; PSRs B1639+36A and B1639+36B. PSR J1717+4308A in M92 is the only known pulsar in that cluster, and has an accurate position and is detected in LoTSS DR2. See Sect. 3.2 for the non-detection of the pulsars in M3 and M13.

No radio pulsars are known in Ko 2, Pal 4, NGC 2419 and NGC 5466³. As these 4 globular clusters have lower central luminosity densities ($\rho_0 = 10^{0.1-1.6} L_\odot \text{pc}^{-3}$; [Harris 1996](#)) compared to M3, M13 and M92 ($\rho_0 = 10^{3.5-4.3} L_\odot \text{pc}^{-3}$), the lower stellar density and hence lower stellar encounter rate would predict that fewer neutron stars would be created due to dynamical interactions in these clusters ([Verbunt & Freire 2014](#)). Additionally, Ko 2, Pal 4, NGC 2419 and NGC 5466 are more distant ($d = 16$ to 83 kpc) than M3, M13 and M92 ($d = 7$ to 10 kpc), and hence any radio pulsars in those clusters would be fainter.

Unidentified LoTSS point sources in or near globular clusters may correspond to unlocalized or even undiscovered radio pulsars. We do not detect any sources within the half-light radii of globular clusters Ko 2, Pal 4 and M3. Figure 3 shows the LoTSS images and catalogued sources in NGC 2419, NGC 5466, M13 and M92, for which sources are detected within the half-light radii from [Harris \(1996\)](#). These clusters are also covered in VLITE commensal continuum imaging observations by [McCarver et al. \(2024\)](#) at 340 MHz (NGC 2419 and NGC 5466), deep targeted VLA continuum observations by [Shishkovsky et al. \(2020\)](#) at 5.0 and 7.2 GHz (M3, M13 and M92) and X-ray observations with Chandra/ACIS ([Bahramian et al. 2020](#)) (M13, M92). We do not consider ILT J073804.85+385302.8 in NGC 2419, ILT J140527.79+283217.3 and J140533.42+283117.3 in NGC 5466 and ILT J171705.77+430856.7 in M92 as these are resolved sources in LoTSS. We note that the latter corresponds to M92-VLA1 from [Shishkovsky et al. \(2020\)](#).

The unresolved LoTSS source ILT J073809.79+385209.9 in NGC 2419 has no counterparts at other radio frequencies or in X-rays, and the [McCarver et al. \(2024\)](#) non-detection is not constraining the spectral index. No pulsars have been reported by [Lian et al. \(2025\)](#) using targeted time-domain periodicity search with FAST ($S_{1400} > 1.59 \mu\text{Jy}$). ILT J140527.71+283059.9 in NGC 5466 is unresolved and detected at 340 MHz as VLITE-A J140527.6+283100 by [McCarver et al. \(2024\)](#), who have used the LoTSS DR2 flux density to show it has a flat spectrum ($\alpha = -0.1 \pm 0.5$). The unresolved source ILT J164137.13+362633.6 in M13 matches M13-VLA4 and the $S_{144} = 0.77 \pm 0.19$ mJy LoTSS flux density is consistent with the $\alpha = -0.94 \pm 0.31$ spectral index determined from the 5.0 and 7.2 GHz VLA detections by [Shishkovsky et al. \(2020\)](#). With $\alpha = -2.74 \pm 0.44$, M92-VLA12 has one of the steepest spectral indices from the [Shishkovsky et al. \(2020\)](#) sample and would have $S_{144} > 90$ mJy in LoTSS. Instead, it is detected at $S_{144} = 1.0 \pm 0.2$ mJy as ILT J171702.96+430803.0, suggesting the spectrum is significantly flatter ($\alpha \sim -1.1$) or follows a broken power-law. Hence, none of these unresolved sources have (known) spectral indices

that would suggest they would be promising targets for targeted pulsar periodicity searches. The lack of X-ray counterparts to these radio sources supports this.

The absence of LoTSS counterparts to the radio sources reported by [Shishkovsky et al. \(2020\)](#) at 5.0 and 7.2 GHz located within the half-light radii of M3, M13 and M92 indicates that if these sources would have power-law spectra, these would have to be relatively shallow, with $\alpha \gtrsim -1.5$, and mostly inconsistent with those of radio pulsars whose spectra follow a distribution with $\alpha = -1.6 \pm 1.0$ ([Jankowski et al. 2018](#)). Continuum observations at intermediate frequencies would be required to rule out broken power-law or curved spectral models.

4. Discussion and conclusions

4.1. Recovery fraction

Figure 4 compares the sensitivity limits and frequency coverage of several time domain pulsar surveys and wide field image domain surveys against observed flux densities of the radio pulsar population from the pulsar catalog. At observing frequencies around 150 MHz, survey sensitivity of the LoTSS image-domain survey should allow for the detection of all known radio pulsars with flux density measurements at that frequency. While the sensitivity limits of time-domain pulsar surveys at L-band frequencies with the large Arecibo (PALFA; [Cordes et al. 2006](#)) and FAST telescopes (GPPS; [Han et al. 2021](#)) are almost an order of magnitude lower than that of LoTSS, the typically steep radio spectra of pulsars (e.g. $S_\nu \propto \nu^\alpha$ with $\alpha = -1.6 \pm 1.0$; [Jankowski et al. 2018](#)) would result in 150 MHz flux densities above the LoTSS sensitivity limit for the majority of the observed pulsar flux density distributions at higher frequencies and over a significant range of power-law spectral indices. As such, we would expect that the majority of radio pulsars would be detectable in LoTSS continuum imaging.

This is confirmed by our catalog matching, as we find that of the 95 pulsars located within the DR2 footprint for which their catalogued positional information allows unambiguous matching, 80 pulsars are recovered in LoTSS. Of the 15 pulsars that were not recovered, there are valid reasons for their non-detection, either due to the pulsars being radio quiet (2 cases), known to be faint at higher frequencies (8 cases) or being RRATs that have low integrated flux densities due to their occasional bright pulses (3 cases). Only in two cases (PSRs J1048+5349 and J2307+2225) were non-detections unexpected.

As a result, we recover over 86% (up to 97% when accounting for pulsars which are known RRATs, radio-quiet and/or faint) of the radio pulsars with accurate locations (better than $20''$) that coincide with the LoTSS DR2 footprint. At 150 MHz, this fraction can be compared to the 23% recovery fraction (288 out of 1238) of [Frail et al. \(2016\)](#) using the TGSS ADR1 image-domain survey ([Intema et al. 2017](#)) and 8% (83 out of 1000) from ([Sett et al. 2024](#)) with the MWA telescope (SMART survey; [Bhat et al. 2023](#)) due to their higher (3-8 mJy) sensitivity limits. At higher frequencies, 661 out of 2235 known radio pulsars (30%) were recovered in the RACS survey with ASKAP at 888 MHz ([Anumalapudi et al. 2023](#)), while the NVSS survey at 1.4 GHz recovered 79 of the 516 radio pulsars (15%) known at the time ([Kaplan et al. 1998](#)).

Conservatively, 51 of the detected pulsars are bright enough ($S_{144} \geq 4$ mJy) to surpass the sensitivity of LoTSS in polarized emission ([O'Sullivan et al. 2023](#), [Callingham et al. 2023](#)). We find that the resulting fraction of pulsars that are detectable in polarized emission of 68% is high compared to the 48% obtained

³ <https://www3.mpi-fr-bonn.mpg.de/staff/pfreire/GCpsr.html>

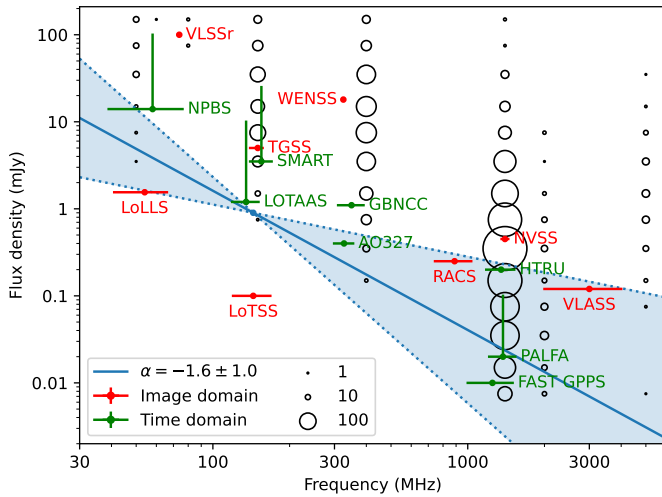


Fig. 4. A comparison of survey sensitivity and frequency coverage of various time domain pulsar surveys (green) and wide area continuum image domain surveys (red) against distributions of pulsar flux density measurements from the pulsar catalog (open circles). An example power law spectrum $S_\nu \propto \nu^\alpha$ with $\alpha = -1.6 \pm 1.0$ for $S_{144} = 0.9$ mJy is shown for reference. (References: NPBS; Brionne et al. 2025, LOTAAS; Sanidas et al. 2019, SMART; Bhat et al. 2023, AO327; Deneva et al. 2013, GBNCC; Stovall et al. 2014, FAST GPPS; Han et al. 2021, PALFA; Cordes et al. 2006, HTRU; Keith et al. 2010, LoLLS; de Gasperin et al. 2021a, VLSSr; Lane et al. 2014, LoTSS; Shimwell et al. 2017, TGSS; Intema et al. 2017, WENSS; Rengelink et al. 1997, RACS; McConnell et al. 2020, NVSS; Condon et al. 1998, VLASS; Lacy et al. 2020).

by Frail et al. (2024) in the MeerKAT survey of the Galactic bulge at L-band, where we note that Frail et al. (2024) includes a larger number of false positives in their matches. Polarization leakage is similar for all polarization types (Shimwell et al. 2022, Taylor et al. 2024), and polarization fractions for which a source is considered polarized are similar between Frail et al. (2024), O’Sullivan et al. (2023) and Callingham et al. (2023).

4.2. Flux densities

Following the definition and recommendation from (Shimwell et al. 2022) separating resolved from unresolved sources based on the ratio between integrated flux density and peak brightness, we find that the properties of the pulsars catalogued in LoTSS DR2 are all consistent with being unresolved. Since none of the matched pulsars are known to be associated with supernova remnants or pulsar wind nebulae, this matches expectations. Conversely, the measured flux densities represent the phase averaged pulsar emission and will not be skewed by radio emission from supernova remnants or pulsar wind nebulae (e.g. Frail et al. 2016).

Due to the long integration times (8 h) and observing bandwidth (48 MHz) used by LoTSS, the LoTSS observations are robust against scintillation, as scintillation generally occurs on timescales and bandwidths on the order of minutes in duration and several kHz to a MHz in bandwidth (e.g. Wu et al. 2022). As a result, the LoTSS flux densities generally match literature values, with the exception of PSRs B0823+26 and J0218+4232.

The former is a known pulsar which displays long nulls – the temporary absence of pulsations – on timescales of minutes to hours (Young et al. 2012; Sobey et al. 2015). As a result, flux density measurements are impacted by the behaviour of the pul-

sar during observations, leading to large variations in the integrated flux density between observations. PSR J0218+4232 is a millisecond pulsar ($P = 2.3$ ms, $DM = 61.25$ pc cm $^{-3}$) which is not known to be nulling, and the image-domain flux densities of $S_{144} = 577(87)$ mJy and $S_{150} = 432(43)$ mJy from LoTSS and TGSS ADR1 (Frail et al. 2016; Intema et al. 2017), while consistent with each other, are significantly brighter than the LOFAR time-domain measurement of $S_{150} = 38(19)$ mJy (Kondratiev et al. 2016). While Frail et al. (2016) attributes the difference to scintillation, Kondratiev et al. (2016) argues that the wide phase resolved pulse profile of PSR J0218+4232 could be affected by scattering, resulting in the pulsed flux density being underestimated in comparison to the integrated flux density. Since a significant fraction of the radio emission of PSR J0218+4232 is known to be unpulsed (Navarro et al. 1995; Kuniyoshi et al. 2015) due to the pulsar being an aligned rotator (Stairs et al. 1999), we consider it likely that this – at least partially – explains the large difference between the pulsed and total integrated flux densities.

The loss of pulsed flux due to scatter broadening in time-domain observations is expected at LOFAR frequencies. The sample of 73 newly discovered pulsars and 311 redetected known pulsars in the LOTAAS survey at 135 MHz all have dispersion measures of $DM \lesssim 220$ pc cm $^{-3}$, which is in agreement with sensitivity limits that account for temporal broadening of pulse profiles due to scattering (which approximately scales with dispersion measure) (Sanidas et al. 2019). Since LoTSS DR2 covers high Galactic latitudes, the dispersion measures in our sample are all within that limit, with PSR J2155+2813 having the highest at $DM = 77.13$ pc cm $^{-3}$, and hence for slow pulsars (e.g. $P > 0.1$ s), we do not expect differences between the observed time-domain and image-domain flux densities. For faster spinning pulsars, the effects of scatter broadening can still be significant, as may be the case for PSR J0218+4232. The time-domain flux densities of the other 5 millisecond pulsars (PSRs J1012+5307, J1544+4937, J1816+4510, J2214+3000, J2322+2057) investigated by Kondratiev et al. (2016) are all consistent with the LoTSS image-domain flux densities, and Kondratiev et al. (2016) does not consider their profiles to be scattering dominated. These 5 millisecond pulsars all have longer spin periods, and/or smaller dispersion measurements, compared to PSR J0218+4232 so the effects of scatter broadening would be expected to be less.

4.3. Selection criteria for identifying pulsar candidates

The high sensitivity and spatial resolution of the LoTSS survey offers the possibility of identifying promising pulsar candidates from the continuum sources detected as part of this survey. Given the characteristic properties of pulsars in the image domain as generally unresolved, steep radio spectrum, and linearly and/or circularly polarized sources that lack counterparts at other wavelengths, we use the properties of the sample of known pulsars in LoTSS DR2 to evaluate which properties provide the best means of identifying pulsar candidates.

Since the majority (92%) of the radio sources in LoTSS DR2 are classified as unresolved (Shimwell et al. 2022), a selection based purely using unresolved source properties is not constraining.

The LoTSS survey offers flux density measurements at the center of the observed bandwidth, and hence determining in-band spectra for each radio source is not possible from the current data. As evident from Fig. 4, cross-matching LoTSS source positions to radio sources in other image-domain surveys is

likely leading to detections for LoTSS sources that are bright and/or have a flat spectrum, with only the LoLLS, RACS and VLASS surveys offering the possibility of detecting counterparts to a large range in flux densities at 144 MHz and spectral indices. Of the 80 radio pulsars recovered in LoTSS, only a few have counterparts in the surveys with the VLA that fully cover the LoTSS DR2 footprint, with 2 counterparts at 74 MHz (VLSSr), 4 at 1400 MHz (NVSS), and 3 at 3 GHz (VLASS). Partial coverage is offered by RACS (up to $\delta < 41^\circ$), which has 1 counterpart and WENSS with 2 counterparts. The LOFAR LBA Sky Survey (LoLSS) at 54 MHz is most promising due to its depth of $S_{54} \sim 1 \text{ mJy beam}^{-1}$ (de Gasperin et al. 2021b) and of the 8 known pulsars with accurate positions present in the 650 deg^2 area released in LoLLS DR1 (de Gasperin et al. 2023), 2 are detected (PSRs B1508+55 and J1552+5437), resulting in a 25% recovery fraction. A cross matched catalog between LoLLS at 54 MHz and LoTSS at 144 MHz by Böhme et al. (2023) reveals that the majority (99.5%) of (non-artifact) radio sources in LoLSS have counterparts in LoTSS, with about 1.3% having steep power-law spectral indices ($\alpha < -2$). A selection based on spectral properties between a cross matched catalog of LoLSS and LoTSS radio sources removes the majority of other sources (e.g. radio loud AGN that have typical spectral indices of $\alpha = -0.7$, e.g. Calistro Rivera et al. 2017, Sabater et al. 2019) and would yield hundreds to thousands of candidates. Candidates can be further constrained by removing sources that have been matched to optical counterparts by Hardcastle et al. (2023).

As discussed in Sect. 3.4, the surveys for linearly and circularly polarized emission from LoTSS DR2 sources by O’Sullivan et al. (2023) and Callingham et al. (2023) identified 35 of the 80 known radio pulsars by their polarization properties, making candidate selection based on polarization very promising. Sobey et al. (2022) used this approach on pre-publication data from O’Sullivan et al. (2023) and Callingham et al. (2023) and selected pulsar candidates from linearly polarized sources with $S_{144} > 2 \text{ mJy}$ and $> 7\%$ polarization fraction and circularly polarized sources with $S_{144} > 5 \text{ mJy}$ and $> 1\%$ polarization fraction that were unresolved in Stokes I and did not have multi-wavelength counterparts that would identify them as likely galaxies. This yielded 9 linearly polarized candidates of which 3 were identified as radio pulsars, and 21 circularly polarized candidates, 5 of which were identified as radio pulsars.

Based on these results, selecting pulsar candidates based on polarization properties is the most promising approach to find new pulsars from wide-area image-domain surveys, though we expect that cross-matching LOFAR radio sources from LoLSS at 54 MHz with LoTSS at 144 MHz to select based on spectral properties will result in additional pulsar candidates, and provide some bias against pulsars that do not appear polarized. These approach matches that suggested by Sett et al. (2023) based on studies with the MWA.

4.4. Outlook

The upcoming LoTSS DR3 release (Shimwell et al., in prep.) will cover the full Northern hemisphere above declination $\delta > 0^\circ$ at 120–168 MHz and will include the Galactic plane to offer coverage of another 1330 known radio pulsars, of which some 870 have accurate positional information in PSRCAT (v2.2.0). The recovery rate of known pulsars in the Galactic plane likely will be lower compared to LoTSS DR2, due to deep time-domain Galactic plane surveys at with the large Arecibo and FAST telescopes (Cordes et al. 2006; Han et al. 2021), as their L-band sensitivities are high enough that only relatively steep pulsar spectra

($\alpha \lesssim -1.7$) are detectable with LoTSS at 144 MHz. Additionally, the presence of resolved and diffuse structures such as supernova remnants, H II regions and pulsar wind nebulae at low Galactic latitudes may impact the calibration of LoTSS visibilities, leading to reduced image fidelity.

Since pulsars at lower Galactic latitudes can have dispersion measures in excess of $\text{DM} \gtrsim 220 \text{ pc cm}^{-3}$, where scatter broadening at radio frequencies near 150 MHz is observed to completely smear out pulsations of even non-recycled pulsars ($P \sim 1 \text{ s}$; Sanidas et al. 2019) in time-domain observations, the LoTSS image-domain survey would provide crucial flux density measurements to assess pulsar spectra of a large sample of radio pulsars at 144 MHz.

Additionally, the LOFAR LBA Sky Survey (LoLSS) will cover the Northern hemisphere above declination $\delta > 24^\circ$ in the 41–66 MHz frequency range (de Gasperin et al. 2021a), and once released will provide additional flux density measurements and, when combined with LoTSS detections, image-based spectral measurements. Together, the complete LoTSS and LoLSS surveys will provide a unique dataset to investigate the spectral properties of radio pulsars as well as select pulsar candidates for time-domain follow up observations.

Acknowledgements. JRC acknowledges funding from the European Union via the European Research Council (ERC) grant Epaphus (project number 101166008). This paper made extensive use of the Python scientific software stack (Pérez et al. 2011), and we acknowledge the developers of *numpy* (van der Walt et al. 2011), *matplotlib* (Hunter 2007), *psrqpy* (Pitkin 2018), *scipy* (Virtanen et al. 2020), *astropy* (Astropy Collaboration et al. 2013, 2018, 2022), *aplpy* (Robitaille & Bressert 2012, Robitaille 2019), *MOC* (Fernique et al. 2014) and *astroquery* (Ginsburg et al. 2019).

References

- Abdollahi, S., Acero, F., Baldini, L., et al. 2022, *ApJS*, 260, 53
- Afzal, A., Agazie, G., Anumalapudi, A., et al. 2023, *ApJ*, 951, L11
- Anumalapudi, A., Ehleke, A., Jones, M. L., et al. 2023, *ApJ*, 956, 28
- Astropy Collaboration, Price-Whelan, A. M., Lim, P. L., et al. 2022, *ApJ*, 935, 167
- Astropy Collaboration, Price-Whelan, A. M., Sipőcz, B. M., et al. 2018, *AJ*, 156, 123
- Astropy Collaboration, Robitaille, T. P., Tollerud, E. J., et al. 2013, *A&A*, 558, A33
- Backer, D. C., Kulkarni, S. R., Heiles, C., Davis, M. M., & Goss, W. M. 1982, *Nature*, 300, 615
- Bahramian, A., Strader, J., Miller-Jones, J. C. A., et al. 2020, *ApJ*, 901, 57
- Bassa, C. G., Pleunis, Z., Hessels, J. W. T., et al. 2017, *ApJ*, 846, L20
- Bhat, N. D. R., Swainston, N. A., McSweeney, S. J., et al. 2023, *PASA*, 40, e020
- Bilous, A. V., Kondratiev, V. I., Kramer, M., et al. 2016, *A&A*, 591, A134
- Böhme, L., Schwarz, D. J., de Gasperin, F., Röttgering, H. J. A., & Williams, W. L. 2023, *A&A*, 674, A189
- Brionne, M., Griefmeier, J. M., Cognard, I., et al. 2025, *A&A*, 693, A96
- Brylyakova, E. A. & Tyul’bashev, S. A. 2021, *A&A*, 647, A191
- Calistro Rivera, G., Williams, W. L., Hardcastle, M. J., et al. 2017, *MNRAS*, 469, 3468
- Callingham, J. R., Shimwell, T. W., Vedantham, H. K., et al. 2023, *A&A*, 670, A124
- CHIME/Pulsar Collaboration, Amiri, M., Bandura, K. M., et al. 2021, *ApJS*, 255, 5
- Condon, J. J., Cotton, W. D., Greisen, E. W., et al. 1998, *AJ*, 115, 1693
- Cordes, J. M., Freire, P. C. C., Lorimer, D. R., et al. 2006, *ApJ*, 637, 446
- Cordes, J. M. & McLaughlin, M. A. 2003, *ApJ*, 596, 1142
- Cruces, M., Champion, D. J., Li, D., et al. 2021, *MNRAS*, 508, 300
- de Gasperin, F., Edler, H. W., Williams, W. L., et al. 2023, *A&A*, 673, A165
- de Gasperin, F., Williams, W. L., Best, P., et al. 2021a, *A&A*, 648, A104
- de Gasperin, F., Williams, W. L., Best, P., et al. 2021b, *A&A*, 648, A104
- Demorest, P. B. & Goss, W. M. 2024, *Journal of Astronomical History and Heritage*, 27, 465
- Deneva, J. S., Stovall, K., McLaughlin, M. A., et al. 2013, *ApJ*, 775, 51
- Dong, F. A., Crowter, K., Meyers, B. W., et al. 2023, *MNRAS*, 524, 5132
- EPTA Collaboration, InPTA Collaboration, Antoniadis, J., et al. 2023, *A&A*, 678, A50
- Faucher-Giguère, C.-A. & Kaspi, V. M. 2006, *ApJ*, 643, 332

- Fernique, P., Boch, T., Donaldson, T., et al. 2014, MOC - HEALPix Multi-Order Coverage map Version 1.0, IVOA Recommendation 02 June 2014
- Fiore, W., Levin, L., McLaughlin, M. A., et al. 2023, *ApJ*, 956, 40
- Fonseca, E., Cromartie, H. T., Pennucci, T. T., et al. 2021, *ApJ*, 915, L12
- Frail, D. A., Jagannathan, P., Mooley, K. P., & Intema, H. T. 2016, *ApJ*, 829, 119
- Frail, D. A., Polisensky, E., Hyman, S. D., et al. 2024, *ApJ*, 975, 34
- Ginsburg, A., Sipőcz, B. M., Brasseur, C. E., et al. 2019, *AJ*, 157, 98
- Graber, V., Ronchi, M., Pardo-Araujo, C., & Rea, N. 2024, *ApJ*, 968, 16
- Haberl, F. 2007, *Ap&SS*, 308, 181
- Han, J. L., Wang, C., Wang, P. F., et al. 2021, *Research in Astronomy and Astrophysics*, 21, 107
- Hardcastle, M. J., Horton, M. A., Williams, W. L., et al. 2023, *A&A*, 678, A151
- Harris, W. E. 1996, *AJ*, 112, 1487
- Hessels, J. W. T., Ransom, S. M., Stairs, I. H., et al. 2006, *Science*, 311, 1901
- Hunter, J. 2007, *Computing in Science Engineering*, 9, 90
- Intema, H. T., Jagannathan, P., Mooley, K. P., & Frail, D. A. 2017, *A&A*, 598, A78
- Jankowski, F., van Straten, W., Keane, E. F., et al. 2018, *MNRAS*, 473, 4436
- Jelić, V., de Bruyn, A. G., Pandey, V. N., et al. 2015, *A&A*, 583, A137
- Jennison, R. C. 1958, *MNRAS*, 118, 276
- Kaplan, D. L., Condon, J. J., Arzoumanian, Z., & Cordes, J. M. 1998, *ApJS*, 119, 75
- Keane, E. F. & McLaughlin, M. A. 2011, *Bulletin of the Astronomical Society of India*, 39, 333
- Keith, M. J., Jameson, A., van Straten, W., et al. 2010, *MNRAS*, 409, 619
- Keith, M. J., Johnston, S., Karastergiou, A., et al. 2024, *MNRAS*, 530, 1581
- Kondratiev, V. I., McLaughlin, M. A., Lorimer, D. R., et al. 2009, *ApJ*, 702, 692
- Kondratiev, V. I., Verbiest, J. P. W., Hessels, J. W. T., et al. 2016, *A&A*, 585, A128
- Kulkarni, S. R. 2024, *Journal of Astronomical History and Heritage*, 27, 482
- Kuniyoshi, M., Verbiest, J. P. W., Lee, K. J., et al. 2015, *MNRAS*, 453, 828
- Lacy, M., Baum, S. A., Chandler, C. J., et al. 2020, *PASP*, 132, 035001
- Lane, W. M., Cotton, W. D., van Velzen, S., et al. 2014, *MNRAS*, 440, 327
- Lewandowski, W., Wolszczan, A., Feiler, G., Konacki, M., & Sołtysiński, T. 2004, *ApJ*, 600, 905
- Lewis, E. F., Olszanski, T. E. E., Deneva, J. S., et al. 2023, *ApJ*, 956, 132
- Lian, Y., Pan, Z., Zhang, H., et al. 2025, *ApJS*, 279, 51
- Lorimer, D. R. & Kramer, M. 2004, *Handbook of Pulsar Astronomy*, Vol. 4
- Lorimer, D. R. & Kramer, M. 2012, *Handbook of Pulsar Astronomy*
- Lynch, R. S., Swiggum, J. K., Kondratiev, V. I., et al. 2018, *ApJ*, 859, 93
- Main, R. A., Parthasarathy, A., Johnston, S., et al. 2023, *MNRAS*, 518, 1086
- Manchester, R. N., Hobbs, G. B., Teoh, A., & Hobbs, M. 2005, *AJ*, 129, 1993
- McCarver, A. V., Maccarone, T. J., Ransom, S. M., et al. 2024, *ApJ*, 969, 30
- McConnell, D., Hale, C. L., Lenc, E., et al. 2020, *PASA*, 37, e048
- McKenna, D. 2024, PhD thesis, University of Dublin Trinity College, Ireland
- McKenna, D. J., Keane, E. F., Gallagher, P. T., & McCauley, J. 2024, *MNRAS*, 527, 4397
- McLaughlin, M. A., Lyne, A. G., Lorimer, D. R., et al. 2006, *Nature*, 439, 817
- Michilli, D., Bassa, C., Cooper, S., et al. 2020, *MNRAS*, 491, 725
- Navarro, J., de Bruyn, A. G., Frail, D. A., Kulkarni, S. R., & Lyne, A. G. 1995, *ApJ*, 455, L55
- O'Sullivan, S. P., Shimwell, T. W., Hardcastle, M. J., et al. 2023, *MNRAS*, 519, 5723
- Pitkin, M. 2018, *Journal of Open Source Software*, 3, 538
- Posselt, B., Karastergiou, A., Johnston, S., et al. 2023, *MNRAS*, 520, 4582
- Pérez, F., Granger, B. E., & Hunter, J. D. 2011, *Computing in Science & Engineering*, 13, 13
- Ransom, S. M., Eikenberry, S. S., & Middleditch, J. 2002, *AJ*, 124, 1788
- Readhead, A. C. S. 2024, *Journal of Astronomical History and Heritage*, 27, 453
- Reardon, D. J., Zic, A., Shannon, R. M., et al. 2023, *ApJ*, 951, L6
- Rengelink, R. B., Tang, Y., de Bruyn, A. G., et al. 1997, *A&AS*, 124, 259
- Robitaille, T. 2019, *APLpy v2.0: The Astronomical Plotting Library in Python*
- Robitaille, T. & Bressert, E. 2012, *APLpy: Astronomical Plotting Library in Python*, *Astrophysics Source Code Library*, record ascl:1208.017
- Ryle, M. & Hewish, A. 1960, *MNRAS*, 120, 220
- Sabater, J., Best, P. N., Hardcastle, M. J., et al. 2019, *A&A*, 622, A17
- Sanidas, S., Cooper, S., Bassa, C. G., et al. 2019, *A&A*, 626, A104
- Sett, S., Bhat, N. D. R., Sokolowski, M., & Lenc, E. 2023, *PASA*, 40, e003
- Sett, S., Sokolowski, M., Lenc, E., & Bhat, N. D. R. 2024, *PASA*, 41, e045
- Shimwell, T. W., Hardcastle, M. J., Tasse, C., et al. 2022, *A&A*, 659, A1
- Shimwell, T. W., Röttgering, H. J. A., Best, P. N., et al. 2017, *A&A*, 598, A104
- Shishkovsky, L., Strader, J., Chomiuk, L., et al. 2020, *ApJ*, 903, 73
- Smirnova, T. V., Tyul'bashev, S. A., Brylyakova, E. A., et al. 2022, *MNRAS*, 517, 1126
- Smith, D. A., Abdollahi, S., Ajello, M., et al. 2023, *ApJ*, 958, 191
- Sobey, C., Bassa, C. G., O'Sullivan, S. P., et al. 2022, *A&A*, 661, A87
- Sobey, C., Bilous, A. V., Griebmeier, J. M., et al. 2019, *MNRAS*, 484, 3646
- Sobey, C., Young, N. J., Hessels, J. W. T., et al. 2015, *MNRAS*, 451, 2493
- Stairs, I. H. 2003, *Living Reviews in Relativity*, 6, 5
- Stairs, I. H., Thorsett, S. E., & Camilo, F. 1999, *ApJS*, 123, 627
- Stovall, K., Lynch, R. S., Ransom, S. M., et al. 2014, *ApJ*, 791, 67
- Tan, C. M., Bassa, C. G., Cooper, S., et al. 2020, *MNRAS*, 492, 5878
- Taylor, A. R., Sekhar, S., Heino, L., et al. 2024, *MNRAS*, 528, 2511
- Turner, J. D., Stappers, B. W., Tian, J., et al. 2025, *MNRAS*, 537, 1070
- Tyul'bashev, S. A., Tyul'bashev, V. S., Kitaeva, M. A., et al. 2017, *Astronomy Reports*, 61, 848
- Tyul'bashev, S. A., Tyul'bashev, V. S., Malofeev, V. M., et al. 2018, *Astronomy Reports*, 62, 63
- van der Walt, S., Colbert, S., & Varoquaux, G. 2011, *Computing in Science Engineering*, 13, 22
- van der Wateren, E., Bassa, C. G., Cooper, S., et al. 2023, *A&A*, 669, A160
- van Haarlem, M. P., Wise, M. W., Gunst, A. W., et al. 2013, *A&A*, 556, A2
- Verbunt, F. & Freire, P. C. C. 2014, *A&A*, 561, A11
- Virtanen, P., Gommers, R., Oliphant, T. E., et al. 2020, *Nature Methods*, 17, 261
- Wang, L., Peng, B., Stappers, B. W., et al. 2020, *ApJ*, 892, 43
- Wu, Q. D., Yuan, J. P., Wang, N., et al. 2023, *MNRAS*, 522, 5152
- Wu, Z., Verbiest, J. P. W., Main, R. A., et al. 2022, *A&A*, 663, A116
- Xu, H., Chen, S., Guo, Y., et al. 2023, *Research in Astronomy and Astrophysics*, 23, 075024
- Young, N. J., Stappers, B. W., Weltevrede, P., Lyne, A. G., & Kramer, M. 2012, *MNRAS*, 427, 114

Appendix A: Pulsars detected in LoTSS DR2

Table A.1. Properties of pulsars and their matching source from LoTSS.

Pulsar	Pol.	P (ms)	DM (pc/cc)	ILT	$\Delta\alpha$ ($''$)	$\Delta\delta$ ($''$)	S_{144} (mJy)	Field
J0006+1834		694	11	J000604.63+183455.7	+2 $^{\circ}$ 43(3 $^{\circ}$ 03)	+3 $^{\circ}$ 28(4 $^{\circ}$ 02)	7.0(1.2)	P002+18
J0039+3546		537	53	J003908.81+354616.7	+0 $^{\circ}$ 04(0 $^{\circ}$ 25)	−0 $^{\circ}$ 35(0 $^{\circ}$ 26)	5.5(0.8)	P009+36
B0045+33	V	1217	40	J004833.97+341207.4	+0 $^{\circ}$ 13(0 $^{\circ}$ 51)	+0 $^{\circ}$ 61(0 $^{\circ}$ 34)	20.7(3.1)	P013+34
J0146+3055		938	25	J014640.97+305520.3	+0 $^{\circ}$ 72(0 $^{\circ}$ 60)	−1 $^{\circ}$ 23(0 $^{\circ}$ 52)	3.8(0.6)	P027+31
J0154+1833	L	2.365	20	J015436.89+183350.8	−0 $^{\circ}$ 04(0 $^{\circ}$ 32)	−0 $^{\circ}$ 19(0 $^{\circ}$ 28)	4.2(0.7)	P029+19
B0153+39		1812	59.83	J015654.94+394929.8	+3 $^{\circ}$ 50(4 $^{\circ}$ 51)	−1 $^{\circ}$ 35(3 $^{\circ}$ 25)	5.3(0.8)	P028+41
J0158+2106	L	505	20	J015845.99+210646.7	+0 $^{\circ}$ 10(1 $^{\circ}$ 53)	+0 $^{\circ}$ 29(0 $^{\circ}$ 31)	4.3(0.7)	P029+21
J0218+4232	L ^a	2.323	61.25	J021806.34+423217.4	+0 $^{\circ}$ 25(0 $^{\circ}$ 20)	−0 $^{\circ}$ 11(0 $^{\circ}$ 20)	577.3(86.7)	P035+41
J0220+3626	L/V	1030	40	J022042.12+362655.7	−0 $^{\circ}$ 02(0 $^{\circ}$ 37)	−0 $^{\circ}$ 07(0 $^{\circ}$ 29)	24.5(3.7)	P035+36
J0227+3356		1240	27	— ^b	—	—	2.1(0.4)	P035+34
B0751+32	L/V	1442	40	J075440.65+323156.5	+0 $^{\circ}$ 40(0 $^{\circ}$ 27)	−0 $^{\circ}$ 17(0 $^{\circ}$ 31)	15.1(2.3)	P118+32
J0811+3729		1248	15	J081115.14+372915.0	−0 $^{\circ}$ 52(0 $^{\circ}$ 39)	−1 $^{\circ}$ 27(0 $^{\circ}$ 68)	1.7(0.3)	P122+37
J0815+4611	L ^c	434.2	11	J081559.49+461153.4	−0 $^{\circ}$ 33(0 $^{\circ}$ 26)	−0 $^{\circ}$ 19(0 $^{\circ}$ 26)	10.5(1.6)	P122+47
B0823+26	V	530.7	19	J082651.49+263720.4	+0 $^{\circ}$ 47(0 $^{\circ}$ 38)	+0 $^{\circ}$ 31(0 $^{\circ}$ 43)	44.6(7.3)	P126+27
J0828+5304		14	23	J082825.68+530443.2	+0 $^{\circ}$ 17(0 $^{\circ}$ 25)	−0 $^{\circ}$ 14(0 $^{\circ}$ 26)	4.5(0.7)	P126+52
J0854+5449		1233	18.84	J085425.70+544928.8	+0 $^{\circ}$ 21(0 $^{\circ}$ 30)	−0 $^{\circ}$ 04(0 $^{\circ}$ 32)	1.9(0.3)	P133+55
J0857+3349		243	24	J085707.09+334918.3	−0 $^{\circ}$ 26(0 $^{\circ}$ 43)	−1 $^{\circ}$ 35(0 $^{\circ}$ 68)	2.4(0.4)	P135+34
B0917+63	L/V	1568	13.15	J092114.15+625413.9	−0 $^{\circ}$ 13(0 $^{\circ}$ 24)	−0 $^{\circ}$ 01(0 $^{\circ}$ 28)	10.5(1.6)	P141+62
J0925+6103		5.983	21.64	J092517.58+610304.2	−0 $^{\circ}$ 27(0 $^{\circ}$ 39)	−0 $^{\circ}$ 15(0 $^{\circ}$ 37)	1.5(0.3)	P141+62
J0928+3039		2092	22	J092859.38+303926.9	−0 $^{\circ}$ 20(0 $^{\circ}$ 32)	−0 $^{\circ}$ 44(0 $^{\circ}$ 39)	3.1(0.5)	P141+29
J0935+3312		962	18	J093507.82+331237.1	−0 $^{\circ}$ 32(0 $^{\circ}$ 27)	−0 $^{\circ}$ 53(0 $^{\circ}$ 29)	3.7(0.6)	P142+32
J0944+4106	L	2229	21	J094418.14+410604.1	+0 $^{\circ}$ 02(0 $^{\circ}$ 26)	+0 $^{\circ}$ 37(0 $^{\circ}$ 28)	4.2(0.6)	P146+42
J1012+5307	V	5.256	9.02	J101233.44+530702.2	+0 $^{\circ}$ 00(0 $^{\circ}$ 21)	−0 $^{\circ}$ 10(0 $^{\circ}$ 21)	20.2(3.0)	P151+52
J1017+3011		452.8	27	J101736.30+301146.0	−0 $^{\circ}$ 11(0 $^{\circ}$ 56)	+0 $^{\circ}$ 07(0 $^{\circ}$ 52)	2.5(0.4)	P153+30
J1049+5822	L	727.6	12.36	J104937.86+582217.6	+0 $^{\circ}$ 34(1 $^{\circ}$ 23)	−0 $^{\circ}$ 54(0 $^{\circ}$ 94)	2.0(0.3)	P161+60
J1059+6459		3631	19.3	J105927.36+645932.0	+0 $^{\circ}$ 92(0 $^{\circ}$ 40)	−0 $^{\circ}$ 15(2 $^{\circ}$ 67)	4.2(0.6)	P162+65
B1112+50		1656	9.19	J111537.51+503006.1 ^d	—	—	21(4)	P10Hetdex
J1239+3239	L	4.701	16.86	J123927.33+323923.4	−0 $^{\circ}$ 20(0 $^{\circ}$ 21)	−0 $^{\circ}$ 09(0 $^{\circ}$ 21)	20.6(3.1)	P188+32
J1243+3946		1310	29	J124303.34+394609.7	+1 $^{\circ}$ 91(0 $^{\circ}$ 46)	−0 $^{\circ}$ 53(0 $^{\circ}$ 34)	5.7(0.9)	P191+40
J1303+3815		396	19	J130319.35+381503.2	−0 $^{\circ}$ 06(0 $^{\circ}$ 29)	−0 $^{\circ}$ 10(0 $^{\circ}$ 29)	3.2(0.5)	P197+37
J1327+3423		41.51	4	J132707.56+342337.9	−0 $^{\circ}$ 17(0 $^{\circ}$ 21)	−0 $^{\circ}$ 26(0 $^{\circ}$ 21)	114.3(17.2)	P201+35
J1336+3414		3013	8.5	— ^e	—	—	0.5(0.3)	P204+35
J1343+6634	L	1394	30.03	J134359.33+663425.3	−0 $^{\circ}$ 44(0 $^{\circ}$ 38)	−0 $^{\circ}$ 31(0 $^{\circ}$ 24)	7.6(1.1)	P205+67
J1427+5211		996	25.37	J142707.74+521111.5	−0 $^{\circ}$ 23(0 $^{\circ}$ 37)	+0 $^{\circ}$ 43(0 $^{\circ}$ 36)	2.8(0.5)	P214+52
B1508+55	L	739.7	19.62	J150925.49+553131.7	+0 $^{\circ}$ 61(0 $^{\circ}$ 21)	−0 $^{\circ}$ 17(0 $^{\circ}$ 21)	727.8(109.3)	P227+55
J1518+4904	L/V	40.93	11.61	J151816.80+490434.1	−0 $^{\circ}$ 05(0 $^{\circ}$ 22)	−0 $^{\circ}$ 05(0 $^{\circ}$ 22)	10.3(1.6)	P231+50
J1529+4050		476	7	J152916.53+405057.8	−0 $^{\circ}$ 03(0 $^{\circ}$ 25)	−0 $^{\circ}$ 08(0 $^{\circ}$ 24)	8.4(1.3)	P231+40
J1541+4703		277.7	19.4	J154105.54+470304.0	−0 $^{\circ}$ 04(0 $^{\circ}$ 89)	−0 $^{\circ}$ 39(0 $^{\circ}$ 53)	0.7(0.2)	P236+48
J1544+4937	L/V	2.159	23	J154404.49+493755.3	−0 $^{\circ}$ 02(0 $^{\circ}$ 24)	−0 $^{\circ}$ 01(0 $^{\circ}$ 23)	6.6(1.0)	P235+50
J1552+5437	V	2.428	22.9	J155253.34+543705.6	−0 $^{\circ}$ 04(0 $^{\circ}$ 25)	+0 $^{\circ}$ 14(0 $^{\circ}$ 25)	4.9(0.7)	P236+55
J1602+3901	V	4	17.26	J160218.82+390101.5	+0 $^{\circ}$ 21(1 $^{\circ}$ 22)	+0 $^{\circ}$ 21(0 $^{\circ}$ 93)	26.5(4.2)	P241+40
J1619+3953		1884	23	J161913.40+395306.2	+0 $^{\circ}$ 78(0 $^{\circ}$ 61)	−0 $^{\circ}$ 96(1 $^{\circ}$ 17)	1.5(0.5)	P245+40
J1624+5850		651.8	26.4	J162400.98+585015.8	−0 $^{\circ}$ 11(0 $^{\circ}$ 30)	−0 $^{\circ}$ 09(0 $^{\circ}$ 27)	3.4(0.5)	P246+58
J1628+4406	L/V	181.2	7	J162850.24+440642.5	+0 $^{\circ}$ 71(0 $^{\circ}$ 25)	+0 $^{\circ}$ 09(0 $^{\circ}$ 25)	12.4(1.9)	P247+45
J1630+3550	L	3.229	17	J163035.93+355042.5	+0 $^{\circ}$ 19(0 $^{\circ}$ 28)	−0 $^{\circ}$ 06(0 $^{\circ}$ 28)	5.9(0.9)	P248+35
J1630+3734	L	3.318	14	J163036.45+373441.9	+0 $^{\circ}$ 20(0 $^{\circ}$ 27)	+0 $^{\circ}$ 07(0 $^{\circ}$ 26)	4.3(0.7)	P249+38
J1638+4005		767.7	33	J163816.24+400556.5	+0 $^{\circ}$ 09(0 $^{\circ}$ 32)	−0 $^{\circ}$ 15(0 $^{\circ}$ 27)	3.1(0.5)	P248+40
B1639+36A		10.38	30	J164140.90+362714.2	−0 $^{\circ}$ 38(0 $^{\circ}$ 86)	+0 $^{\circ}$ 65(0 $^{\circ}$ 71)	1.1(0.3)	P249+38
B1639+36B		3.528	29.45	J164140.37+362558.2	+0 $^{\circ}$ 32(0 $^{\circ}$ 64)	+0 $^{\circ}$ 29(0 $^{\circ}$ 47)	1.1(0.3)	P249+38
J1647+6608	L/V	1600	22.55	J164732.46+660821.9	+0 $^{\circ}$ 35(0 $^{\circ}$ 29)	+0 $^{\circ}$ 25(0 $^{\circ}$ 31)	7.6(1.1)	P254+65
J1656+6203		776.2	35.26	J165610.32+620350.6	−0 $^{\circ}$ 23(0 $^{\circ}$ 41)	−0 $^{\circ}$ 20(0 $^{\circ}$ 39)	1.6(0.3)	P253+63
J1657+3304		1570	24	J165750.67+330434.0	+0 $^{\circ}$ 20(0 $^{\circ}$ 31)	−0 $^{\circ}$ 44(0 $^{\circ}$ 30)	3.1(0.5)	P253+33
J1658+3630	L/V	33.03	3	J165826.55+363030.4	−0 $^{\circ}$ 33(0 $^{\circ}$ 22)	−0 $^{\circ}$ 37(0 $^{\circ}$ 22)	29.5(4.5)	P255+38
J1707+3556		160	19	J170702.75+355636.5	−0 $^{\circ}$ 22(0 $^{\circ}$ 29)	−0 $^{\circ}$ 05(0 $^{\circ}$ 29)	4.4(0.7)	P255+35
J1715+4603		548	21	J171543.76+460400.5	+0 $^{\circ}$ 12(0 $^{\circ}$ 95)	−1 $^{\circ}$ 35(1 $^{\circ}$ 06)	0.6(0.3)	P258+45
J1717+4308A		3.16	35	J171706.53+430802.6	−0 $^{\circ}$ 40(0 $^{\circ}$ 55)	+0 $^{\circ}$ 85(1 $^{\circ}$ 03)	1.5(0.4)	P258+43
J1722+3519	L/V	822	24	J172209.51+351918.7	−0 $^{\circ}$ 01(0 $^{\circ}$ 24)	−0 $^{\circ}$ 17(0 $^{\circ}$ 24)	13.9(2.1)	P261+35

Table A.1. continued.

Pulsar	Pol.	P (ms)	DM (pc/cc)	ILT	$\Delta\alpha$ ($''$)	$\Delta\delta$ ($''$)	S_{144} (mJy)	Field
J1741+3855		829	47.22	J174112.34+385510.1	-0 $^{\circ}$ 03(0 $^{\circ}$ 37)	-0 $^{\circ}$ 25(0 $^{\circ}$ 36)	3.3(0.5)	P265+38
J1745+4254		305	38	J174550.14+425438.0	-0 $^{\circ}$ 19(0 $^{\circ}$ 37)	-0 $^{\circ}$ 13(0 $^{\circ}$ 35)	2.5(0.4)	P265+43
J1758+3030	V	947	35	J175825.86+303024.0	+0 $^{\circ}$ 27(0 $^{\circ}$ 41)	-0 $^{\circ}$ 08(0 $^{\circ}$ 66)	16.8(2.6)	P270+30
B1811+40	L/V	931.1	41.56	J181313.20+401339.3	+0 $^{\circ}$ 88(0 $^{\circ}$ 24)	-0 $^{\circ}$ 26(0 $^{\circ}$ 24)	36.5(5.5)	P272+40
J1816+4510	V	3.193	39	J181635.95+451033.9	-0 $^{\circ}$ 13(0 $^{\circ}$ 21)	-0 $^{\circ}$ 06(0 $^{\circ}$ 21)	76.0(11.4)	P273+45
J1821+4147	V	1262	41	J182152.34+414702.6	-0 $^{\circ}$ 00(0 $^{\circ}$ 27)	-0 $^{\circ}$ 12(0 $^{\circ}$ 25)	6.4(1.0)	P276+43
J2155+2813		1609	77	J215515.22+281309.3	+7 $^{\circ}$ 93(0 $^{\circ}$ 33)	+2 $^{\circ}$ 75(0 $^{\circ}$ 36)	4.7(0.7)	P330+28
J2156+2618		498	48	J215623.71+261829.9	-0 $^{\circ}$ 14(0 $^{\circ}$ 53)	+0 $^{\circ}$ 54(0 $^{\circ}$ 64)	1.8(0.4)	P330+26
J2202+2134		498	17.7	J220217.00+213434.0	-0 $^{\circ}$ 27(0 $^{\circ}$ 75)	-0 $^{\circ}$ 47(0 $^{\circ}$ 58)	4.5(0.8)	P331+21
J2204+2700		84.7	35	J220443.71+270054.9	-1 $^{\circ}$ 28(0 $^{\circ}$ 73)	-0 $^{\circ}$ 31(0 $^{\circ}$ 76)	0.9(0.3)	P330+28
J2212+2450	L/V	3.908	25.21	J221227.63+245036.7	-0 $^{\circ}$ 80(0 $^{\circ}$ 32)	+0 $^{\circ}$ 08(0 $^{\circ}$ 29)	8.3(1.3)	P333+26
B2210+29	V	1005	75	J221223.34+293305.4	+0 $^{\circ}$ 07(0 $^{\circ}$ 23)	-0 $^{\circ}$ 11(0 $^{\circ}$ 23)	15.6(2.3)	P333+31
J2214+3000	L	3.119	23	J221438.84+300038.2	+0 $^{\circ}$ 13(0 $^{\circ}$ 29)	-0 $^{\circ}$ 07(0 $^{\circ}$ 28)	4.7(0.7)	P333+31
J2222+2923		281.4	49	J222303.22+292358.9	+0 $^{\circ}$ 05(0 $^{\circ}$ 36)	-0 $^{\circ}$ 32(0 $^{\circ}$ 30)	4.2(0.7)	P336+28
J2227+3038	V	842	20	J222741.77+303820.8	+0 $^{\circ}$ 03(0 $^{\circ}$ 38)	-0 $^{\circ}$ 03(0 $^{\circ}$ 30)	17.0(2.6)	P336+31
J2229+2643	L	2.978	23	J222950.89+264357.4	-0 $^{\circ}$ 17(0 $^{\circ}$ 24)	+0 $^{\circ}$ 15(0 $^{\circ}$ 24)	12.1(1.8)	P338+26
J2234+2114	V	1359	35	J223456.63+211419.3	+0 $^{\circ}$ 18(0 $^{\circ}$ 50)	-0 $^{\circ}$ 55(0 $^{\circ}$ 55)	23.1(3.5)	P340+21
B2303+30		1576	50	J230558.32+310001.2	+0 $^{\circ}$ 06(0 $^{\circ}$ 22)	+0 $^{\circ}$ 00(0 $^{\circ}$ 22)	30.3(4.6)	P345+31
J2306+3124	L	342	46	J230619.22+312420.2	-0 $^{\circ}$ 25(0 $^{\circ}$ 24)	+0 $^{\circ}$ 15(0 $^{\circ}$ 24)	9.1(1.4)	P345+31
B2315+21	L/V	1445	21	J231757.85+214947.1	-0 $^{\circ}$ 08(0 $^{\circ}$ 22)	+0 $^{\circ}$ 84(0 $^{\circ}$ 22)	56.6(8.6)	P348+21
J2322+2057		4.808	13	J232222.35+205702.8	-0 $^{\circ}$ 23(0 $^{\circ}$ 43)	-0 $^{\circ}$ 18(0 $^{\circ}$ 43)	1.6(0.3)	P351+21
J2350+3140		508	39	J235041.19+314047.4	+0 $^{\circ}$ 18(0 $^{\circ}$ 26)	-0 $^{\circ}$ 20(0 $^{\circ}$ 26)	5.3(0.8)	P357+31
J2355+2246		1841	23	J235549.35+224610.6	+6 $^{\circ}$ 25(4 $^{\circ}$ 51)	+6 $^{\circ}$ 38(8 $^{\circ}$ 01)	3.0(0.5)	P000+23

Notes. Pulsars that we detect by cross-matching pulsars from PSRCAT to sources from LoTSS DR2. The left side of the table shows from left to right: the J- or B-name from pulsars, the letters L and/or V to indicate that a pulsar has been detected in linear polarization from O’Sullivan et al. (2023) and/or circular polarization from Callingham et al. (2023), the spin-period (P) of the respective pulsar in milliseconds and the Dispersion Measure (DM) in pc/cc. The right side of the table shows from left to right: the ILTJ-name of LoTSS sources, the separation in R.A. ($\Delta\alpha$), the separation in Dec. ($\Delta\delta$), the flux density at 144 MHz from LoTSS (S_{144}) and the LoTSS field corresponding to the LoTSS counterpart of the pulsar. ^(a) Reported by Navarro et al. 1995 and Sobey et al. (2022), but not detected in O’Sullivan et al. (2023). ^(b) This source is an extended source made up of two point-sources (Fig. 1f). ^(c) Reported by Jelić et al. (2015), but not detected in O’Sullivan et al. (2023). ^(d) This source is not in the LoTSS catalog (Fig. 1i). ^(e) This source is not in the LoTSS catalog (Fig. 1e).